



Stress measurements of deforming olivine at high pressure

Li Li^{a,*}, Donald Weidner^a, Paul Raterron^b, Jiuhua Chen^a, Michael Vaughan^a

^a Department of Geosciences, Mineral Physics Institute, State University of New York at Stony Brook, Stony Brook, NY 11794-2100, USA

^b Laboratoire de Structure et Propriétés de l'État Solide (Associated to CNRS), Université des Sciences et Technologies de Lille, F-59655 Villeneuve d'Ascq Cedex, France

Received 17 April 2003; received in revised form 16 July 2003; accepted 2 September 2003

Abstract

Rheological properties of mantle minerals are critical for understanding the dynamics of the Earth's deep interior. Due to limitations in experimental technique, previous quantitative studies of the rheological properties of mantle minerals are limited to either low pressure or low temperature. The present understanding of mantle flow is mostly inferred from the extrapolation of relatively low-pressure data to mantle high-pressure conditions. However, the effect of pressure (represented by activation volume) on the rheological properties of olivine is still controversial. Therefore, deformation experiments, carried out at mantle pressures, are necessary to understand and model mantle flow. Here we report an experimental study of plastic deformation of San Carlos olivine ($(\text{Mg, Fe})_2\text{SiO}_4$) under upper mantle conditions. Macroscopic differential stress and strain rates have been measured in situ in a large-volume high-pressure apparatus using newly developed techniques. The differential stress at high temperature and high pressure that we measured is significantly lower than that estimated by many currently accepted olivine flow laws. We document the first in situ experimental differential stress results in a multi-anvil press. Our results give direct evidence for a relatively small activation volume (less than $10^{-5} \text{ m}^3 \text{ mol}^{-1}$). This shows that the effect of pressure on dislocation creep is small.

© 2004 Elsevier B.V. All rights reserved.

Keywords: Olivine; Stress; Strain; Dislocation; Pressure; Grain size

1. Introduction

The effect of pressure (P) on viscosity is important in defining the rheological properties of mantle minerals. It is, however, poorly constrained. The structure and dynamics of the Earth are directly linked to the variation of flow properties with depth. Some seismic observations, such as regions of low velocity and high attenuation at the top of asthenosphere, are explained by the effects of water and/or partial melting

(Weidner, 1974). These agents are further implicated in creating the low viscosity asthenosphere. An increase in creep rate by a factor of 2–5 at a given temperature (T) and stress can result from 3 to 10% melt (Kohlstedt and Chopra, 1994). The maximum effect of adding water to the system, that has been observed, is an order of magnitude increase in strain rate for a given stress and temperature (Hirth and Kohlstedt, 1996). However, for an activation volume (V^*) of $20 \text{ cm}^3 \text{ mol}^{-1}$, pressure will decrease the strain rate by a factor of 1000 by a depth of 100 km. Questions, such as the variation of the viscosity of the mantle with depth, can only be addressed by studying the pressure dependence of the rheology of

* Corresponding author. Tel.: +1-631-632-8220;

fax: +1-631-632-8140.

E-mail address: lilli@notes.cc.sunysb.edu (L. Li).

mantle minerals (Poirier, 1985). In addition, the pressure dependence of olivine rheology is also relevant to the mechanism of deep earthquakes since a small pressure strengthening is required for the observed Wadati–Benioff zone seismicity to be bounded by a constant limiting strength (Brodholt and Stein, 1988).

The effect of pressure on the rheological properties of olivine has been a controversial and ambiguous issue for a few decades even with the realization of its importance. The various experimental attempts to measure the activation volume of olivine dislocation creep at high temperature give bimodal results, yielding values of $0\text{--}6\text{ cm}^3\text{ mol}^{-1}$ (Béjina et al., 1997; Jaoul et al., 1983), or $15\text{--}27\text{ cm}^3\text{ mol}^{-1}$ (Green and Borch, 1987; Borch and Green, 1987; Ross et al., 1979; Kohlstedt and Wang, 2001; Karato and Wu, 1993). The lower values of activation volume for high-temperature creep of olivine come from studies of silicon or oxygen diffusion (Béjina et al., 1997). High-pressure dislocation recovery experiments suggest an activation volume between 6 and $11\text{ cm}^3\text{ mol}^{-1}$ (Karato et al., 1993; Kohlstedt et al., 1980). Deformation reports of olivine at high temperature and low pressure ($<300\text{ MPa}$) concluded that activation volumes range from 13 to $27\text{ cm}^3\text{ mol}^{-1}$ (Green and Borch, 1987; Ross et al., 1979; Kohlstedt

and Wang, 2001; Karato and Wu, 1993) while Borch and Green (1987) pointed out that activation volume may decrease with further increase of pressure.

Here we report the results of a relaxation-style deformation experiment, in which differential stresses and strain rates are measured using synchrotron X-radiation in a multi-anvil high-pressure apparatus. Together with our TEM investigations of the run products and our previous studies (Li et al., 2003), we conclude that the observed small effect of pressure on the rheology of olivine is consistent with the lower range of activation volume ($<10\text{ cm}^3\text{ mol}^{-1}$) at high temperature and high pressure.

2. Flow mechanism

In our previous studies (Li et al., 2003; referred to as Li1), we defined the high-pressure flow mechanism of olivine under the same experimental conditions as the current study. In Li1, olivine samples with two grain-sizes were symmetrically placed in the high-pressure cell assembly and deformed at 8 GPa and $T \leq 1473\text{ K}$. The strain rates of the two samples were found to be the same indicating a grain-size independent flow under the assumption that

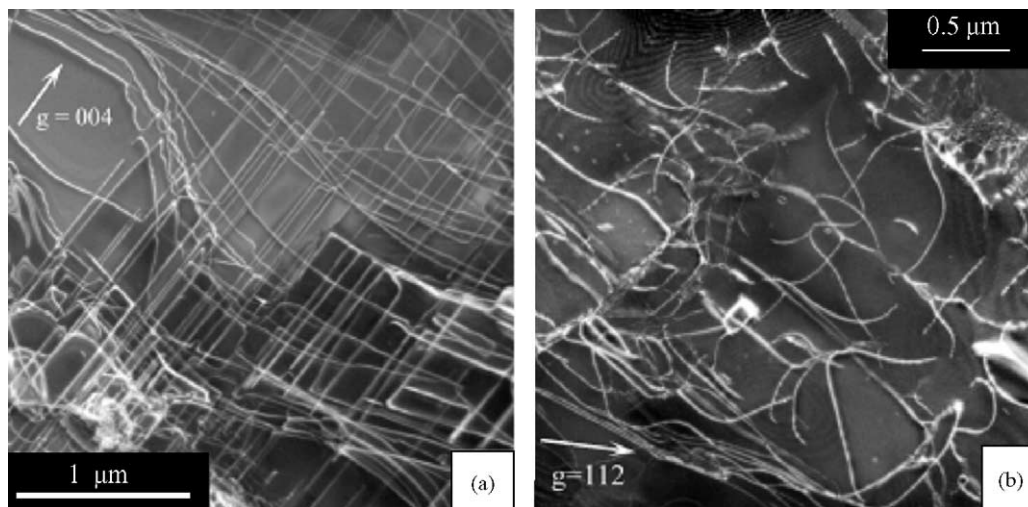


Fig. 1. Dark field weak beam TEM micrographs of olivine dislocation microstructures, comparable in both coarse- and fine-grain materials, here shown in the coarse-grain samples. (a) At 973 K, olivine grains exhibit c dislocations well confined in their glide plane (here (010) plane) with straight screw segments extending throughout the grains and (mobile) curved edge segments. (b) At 1273 K, c dislocations still dominate the deformation although a dislocations are occasionally observed. At that temperature, all dislocation lines are curly and not always confined in their glide plane, which shows that dislocation climb is now an active process.

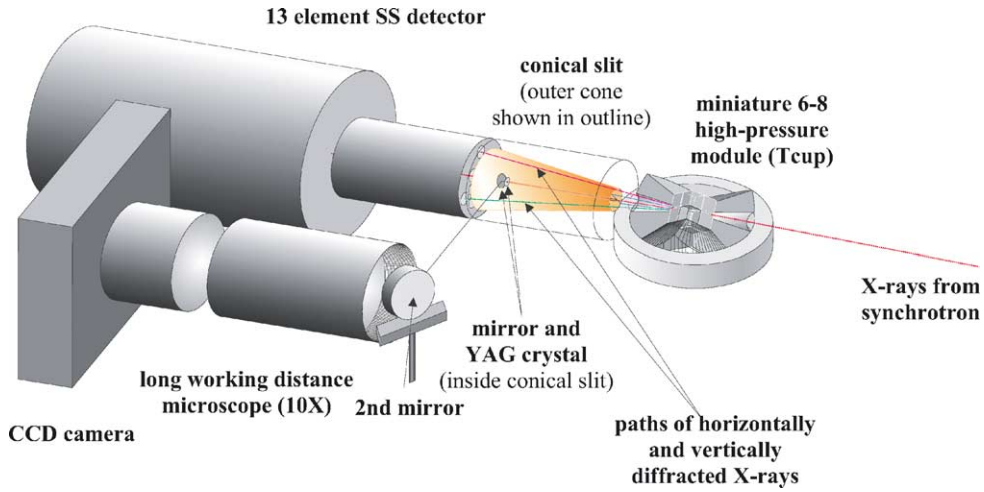


Fig. 2. Multi-anvil high-pressure system. White X-rays from the synchrotron illuminate the sample placed in the T-cup. A conical slit system defines the two theta angle as 6.5° . The collimated diffracted X-ray beams are detected by four elements of a 13-element solid state detector which converts the signals into energy dispersive patterns. A mirror and a fluorescent YAG crystal, mounted inside the conical slit, convert transmitted X-rays into visible light that are recorded by the CCD camera after being magnified by a long working distance microscope.

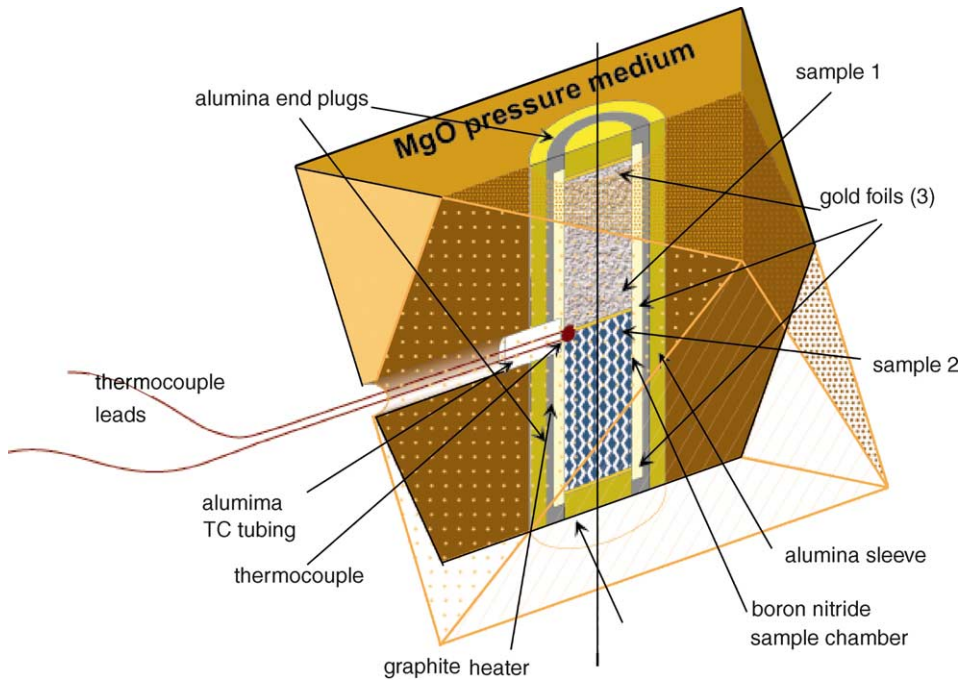


Fig. 3. Schematic cross section of T-cup apparatus cell assembly. An MgO octahedron is used as the pressure medium. A cylindrical furnace is placed inside the MgO octahedron and contains alumina end plugs and two samples symmetrically arranged. The end plugs and the two samples are separated by gold foils, which is used as strain markers. The temperature is measured with a W3%Re–W25%Re thermocouple. Temperature gradients within specimens are less than 10 K mm^{-1} , as calibrated previously in similar cell assemblies.

the arrangement of the sample-cell provides identical stress in the two samples. In the experiment reported here the stresses are measured and the results confirm the assumption of Li1. In the Li1 study, the powder samples were cold pressed to 8 GPa, then heated up to 1473 K in a series of heating steps. In the current study, we followed a similar experimental path as Li1 except we have added an annealing cycle at low pressure (3 GPa). One of the advantages of annealing is that it decreases the effect of X-ray diffraction peak broadening on the differential stress measurement. The microstructures of the Li1 sample at 973, 1273, and 1473 K are reported in Li1. TEM photos (Fig. 1) show the microstructures of the samples annealed at 973 and 1273 K. Li1 concluded that dislocation creep assisted by dynamic recrystallization dominates the flow at T of 1273 and 1473 K at high pressure while low-temperature dislocation glide dominates olivine flow at T of 973 K.

3. Experimental protocol

The current experiment is motivated to measure the differential stress in the deforming sample under high pressure and high temperature. As the procedures for measuring the macroscopic strain rate using X-ray radiography have become routine, we report here a newly developed experimental procedure for measuring the macroscopic differential stress using multiple detectors and anvils transparent to X-rays with a synchrotron X-radiation light source (NSLS). Taken together, these new tools form the basis of these high-pressure rheology studies.

The experiment was performed with a 6–8 double stage multi-anvil high-pressure system, the T-cup (Fig. 2) (Vaughan et al., 1998). Non-hydrostatic stress was produced in the specimens with hard pistons in the cell assembly (Fig. 3). Two separate olivine samples, one with 5 μm average grain size and the other with 0.5 μm average grain size, were separated by a gold foil with additional gold foils between the two samples and the corresponding alumina pistons. The preparation and characterization of the starting samples as well as the evolution of the grain sizes during deformation are described in detail elsewhere (Li1). The water content in the starting material and recovered run product is less than 1 wt. ppm as indicated

by an FTIR investigation performed at the U2A beam line (NSLS). The macroscopic differential stress was measured using multiple energy dispersive detectors, making this the first experiment that directly measures macroscopic differential stress with a large-volume high-pressure system. Cubic boron nitride, which is transparent to X-rays, was used for the second-stage anvils enabling us to simultaneously detect the macroscopic strain and stress, as discussed below. Combin-

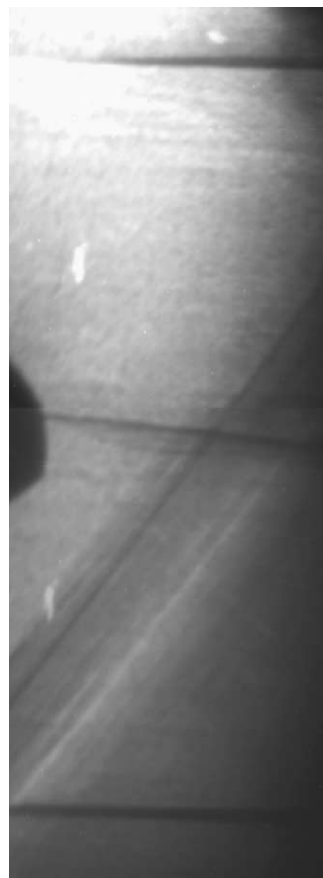


Fig. 4. Magnified digital images, obtained in situ by X-ray radiography, showing the fine (bottom) and coarse (top) grain olivine specimens during Run San_36. The total length of the two samples is about 1.5 mm. The black lines are images of the gold foils which are strain markers. Above and below the samples are the images of the hard-alumina rods used as the pistons in this study. The diagonal features are the shadows of nearly transparent cubic boron nitride anvils. The black blob at the left of the figure is the tip of the thermocouple. The few bright areas in the image are flaws in the fluorescence screen.

ing these techniques, we are able to measure the stress and strain inside the specimen in situ at high P and T as a function of time.

The data reported here are from our experiments performed with SAM85 (Weidner et al., 1992). A white X-ray beam passes through polycrystalline San Carlos olivine samples in the radial direction, and probes the axial and radial lattice strains of the samples as a function of time. At the same time, downstream X-ray radiographic images were captured and magnified (Fig. 4). Gold foils, used as strain markers, are imaged; the resulting images allow the determination of strain to a precision of 10^{-4} (as described in Li1). This yields a precision for strain rate of 10^{-6} s^{-1} for data taken at 100 s intervals or longer. In this experiment, the powder samples were annealed at 3 GPa and 1273 K during the first heating cycle, and were then deformed at 8 GPa at temperatures up to 1473 K. The stress relaxed during the annealing cycle. However, further compression created sufficient differential stress to deform the sample again at 1130 K.

4. Strain analysis

Strain is derived from the comparison of two images created by X-ray radiographs. While the measurement of the absolute length of the sample is accurate to a few pixels, changes in length are measurable to fractions of pixels. The method used here is described in detail in the appendix of Li1.

The results of strain versus time are illustrated in Fig. 5 and documented in Table 1. Strains evolve similarly in the two samples except at temperature equal to 1129 K where the coarse grain sample exhibits higher strains. At temperature of 1504 K or higher, both samples shorten by $\sim 3\%$. The time-resolved strain rates are shown in Fig. 6 and also documented in Table 1. In general, the strain rates of the two samples are the same (except at 1129 K) and decrease with time at each temperature. The data at 1129 K and 8 GPa indicated the onset of measurable flow. At this point, the strength of the material is low enough that stress initiates plastic flow. Strain rate measurements in this study are sparser than in Li1 since experimental time

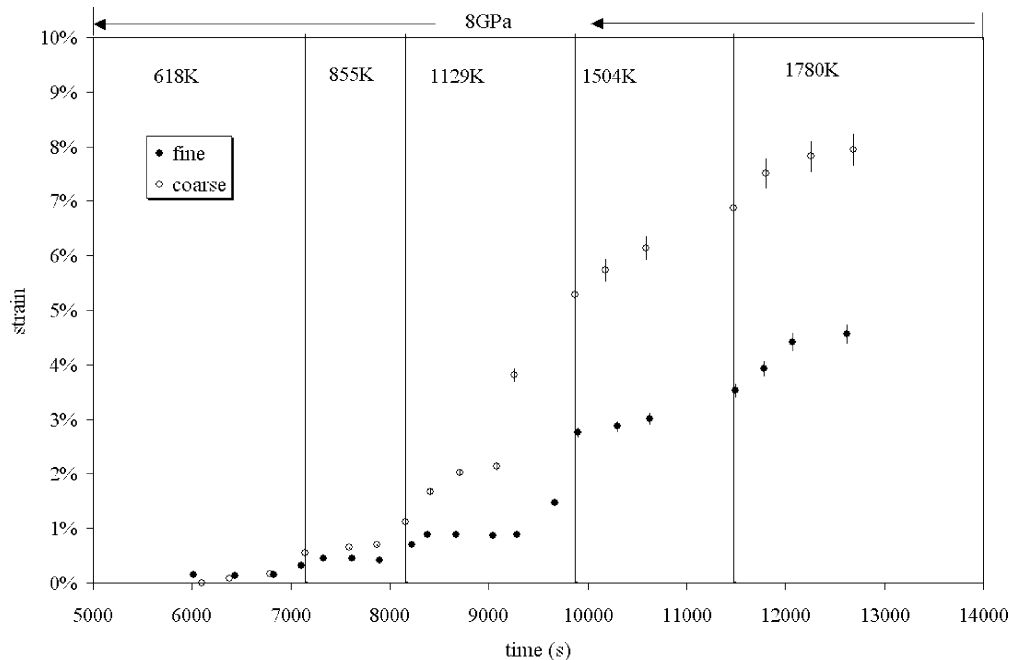


Fig. 5. Time-resolved strain results from Run San_36. The open symbols represent coarse grain sample, the solid symbols represent fine grain sample. Coarse grain sample experienced higher total strain than fine grain sample during the initial yielding period ($T = 1129 \text{ K}$). At higher temperatures, both samples shorten by $\sim 3\%$.

Table 1
Run San_36^a condition, and strain and strain-rate results

P (± 0.5 GPa)	T^b (± 10 K)	Time (± 1 s)	Fine ^c (%)	Fine ^c (10^{-6} s ⁻¹)
8	618	6019	0.1 (0.01)	3.4 (0.4)
8	618	6826	0.2 (0.01)	0.5 (0.7)
8	855	7332	0.5 (0.02)	4.4 (0.6)
8	855	7615	0.5 (0.02)	0.4 (0.6)
8	1129	8386	0.9 (0.03)	6.4 (0.6)
8	1129	8671	0.9 (0.03)	0.2 (0.5)
8	1129	9282	0.9 (0.03)	0.8 (0.5)
8	1504	9901	2.8 (0.1)	33 (0.8)
8	1504	10297	2.9 (0.1)	3.4 (0.6)
8	1504	10623	3.0 (0.1)	1.6 (0.2)
8	1780	11782	3.9 (0.2)	14 (0.7)
8	1780	12068	4.4 (0.2)	8.9 (0.4)
8	1780	12620	4.6 (0.2)	3.1 (0.4)
P (± 0.5 GPa)	T^b (± 10 K)	Time (± 1 s)	Coarse ^c (%)	Coarse ^c (10^{-6} s ⁻¹)
8	618	6786	0.1 (0.03)	2.3 (0.5)
8	855	7590	0.6 (0.02)	3.7 (0.6)
8	855	7867	0.7 (0.02)	1.8 (0.6)
8	1129	8410	1.1 (0.04)	19 (0.7)
8	1129	8706	1.7 (0.06)	9.2 (0.5)
8	1129	9082	2.0 (0.07)	6.6 (1)
8	1504	9871	3.8 (0.1)	48 (1)
8	1504	10176	5.3 (0.2)	11 (0.5)
8	1504	10587	5.7 (0.2)	4.6 (0.3)
8	1780	11805	6.9 (0.3)	14 (0.5)
8	1780	12259	7.5 (0.3)	7.2 (0.5)
8	1780	12689	7.8 (0.3)	2.6 (0.4)

Note. Numbers in parenthesis indicate the one standard deviation.

^a Images of fine and coarse specimens are taken at different times, numbers in the time column are simply converted from hour, minute, and second in the recorded time, then normalized to the starting point of the experiment.

^b W3%Re–W25%Re thermocouple, no pressure correction was applied.

^c Fine and coarse stand for fine- and coarse-powder specimens, respectively. About half of the strains were generated in the first 1000 s at each temperature.

was divided between strain measurements and stress measurements. In the relaxation experiment, strain rates of 10^{-4} s⁻¹ or higher occur in the first 1000 s after each increase in temperature. The measurements in these experiments can be repeated in every 500 s. High strain rate happened during the first 1000 s may not be measured in time. As a result, this approach is limited to investigating deformation experiments with strain rates greater than 10^{-4} s⁻¹.

5. Stress analysis

Macroscopic differential stress manifests, as a uniform lattice strain, when an orientation constrained by

the geometry of our uniaxial deformation cell assembly. Analysis of the lattice strain for an orthorhombic system under non-hydrostatic pressure is described in detail elsewhere (Singh et al., 1998). In summary, lattice strain ε_{ij} and differential stress σ_{ij} is given by Weidner (1998):

$$\varepsilon_{ij} = \sum_{k=1}^3 \sum_{l=1}^3 S_{ijkl} \sigma_{kl} \quad (1)$$

$$\varepsilon_{hkl} = \frac{[d(hkl) - d_p(hkl)]}{d_p(hkl)}$$

where $d(hkl)$ is the d spacing for each hkl , and $d_p(hkl)$ is the d spacing under hydrostatic pressure alone. The elastic compliance tensor, S , is rotated to

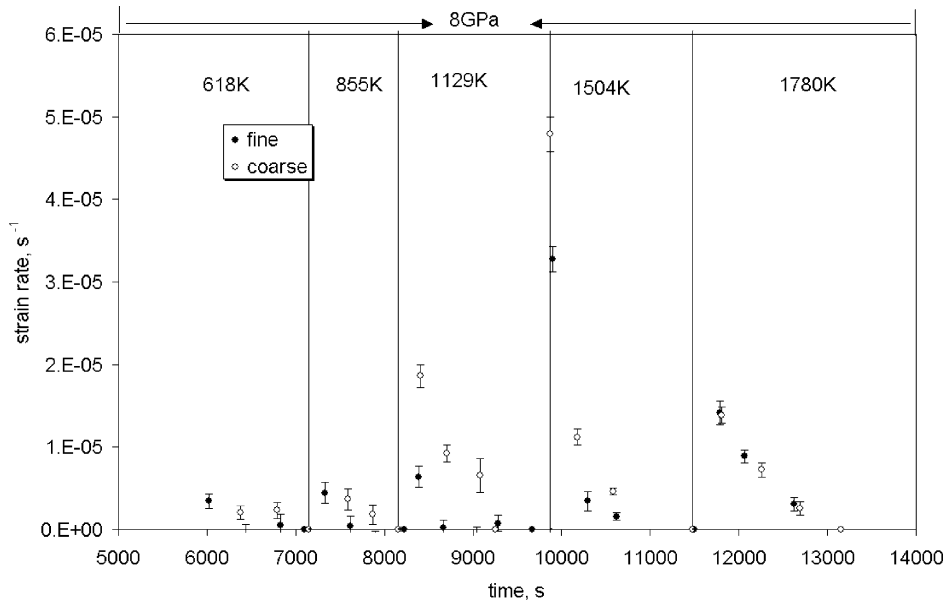


Fig. 6. Time-resolved strain rate results from Run San_36. Open symbols represent coarse grain sample, close symbols represent fine grain sample. Two samples demonstrate very similar flow behavior. At $T < 1100$ K, no significant flow was observed. Significant flow occurs at 1129 K and continues at 1504 and 1780 K. When the temperature is increased, the flow rate is initially high and decays with time as expected in a relaxation style experiment.

the coordinate system of the stress system for each hkl . S in our calculations is from experiment data from Isaak (1992) and Zha et al. (1996).

6. Experimental results

We have measured the macroscopic differential stress as a function of temperature at $P = 8(\pm 0.5)$ GPa. Stress results are illustrated in Fig. 7 and documented in Table 2. Pressure is calculated using the olivine sample itself as the pressure standard with the third-order Birch–Murnaghan equation of state with parameters from Isaak (1992) and Zha et al. (1996). The volume measured after the experiment (quenched and open press) is used as the reference $V_0 (=292.5769 \text{ \AA}^3)$. Stress is determined using Eq. (1) for four different diffraction peaks $\{(112), (130), (131), (021)\}$. The plotted value is for the average of these determinations for the four diffraction peaks, while the range of the individual values is indicated by the error bars. An analysis of the expected error of any one measurement is domi-

nated by the uncertainty in the d spacing resolution and the single-crystal elastic constants at the P , T of the sample and is expected to be less than 0.1 GPa, which is much less than the indicated error bar. On the other hand, the stress defined by each diffraction peak represents the average stress experienced by the subset of grains that contribute to the specific diffraction peak. The grains in any one of these subsets share elastic and plastic properties that may contribute to a unique stress field for the specific subset. As a result the distribution of stress among the different subsets represents the aggregation/stress-distribution process and contributes as the main uncertainty in defining the aggregate stress.

The stresses and the strain rates for the two samples are very similar once plastic flow is initiated ($T > 1129$ K), supporting the assertion that the flow process is grain-size independent. The stress initially increases with heating and reaches the maximum of 1.7 GPa at 875 K and decays rapidly after about 1100 K. The increase in stress with temperature is probably due to the relaxation of the cell assembly on heating.

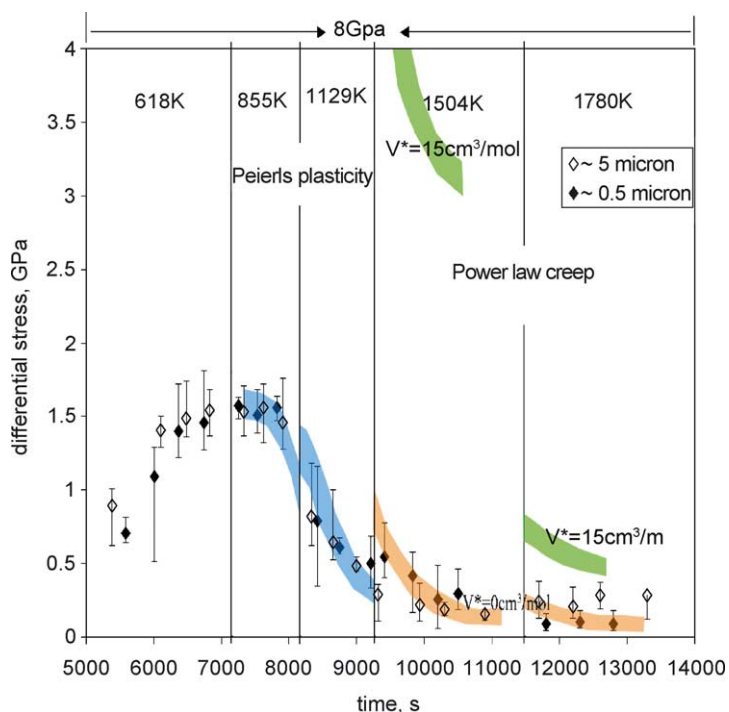


Fig. 7. Macroscopic differential stresses for Run San_36. Measured stresses are represented by either open symbols (for the 5 μm grain size) or solid symbols (for the 0.5 μm grain size). The plotted values are the average of the values of measured stress from diffraction peaks of (1 1 2), (1 3 1), (1 3 0), and (0 2 1). The error bar represents the range of stress values from these four peaks. The colored fields represent the range of stress that is calculated from different flow models at different temperatures as described in Tables 1 and 2 using the strain rate that is given in Fig. 5. The brown region is based on the power law creep flow law parameters given in Table 2 for $V^* = 0 \text{ cm}^3 \text{ mol}^{-1}$. The green region is based on the power law creep flow law parameters given in Table 2 for $V^* = 15 \text{ cm}^3 \text{ mol}^{-1}$. The blue region is based on the Peierls plasticity flow law parameters given in Table 1. The data indicate no grain size sensitivity in either strain rate or stress and are consistent with the literature models only if V^* is small.

7. Discussion and conclusion

Grain-size independent flow dominates the experiments in Li1 and in this study. With the combination of stress and strain rate measurements that are reported here, we have the opportunity to test dry olivine flow laws that have been reported in the literature for a range of activation volumes. In this discussion, we interpret our measurements as steady state data even though they are gathered during a relaxation process. Phenomena such as transient creep are superimposed on and difficult to separate from the steady state process. However, we expect that cold compression will introduce a high dislocation density into the sample and will thus work-harden the sample. This will make the stress field higher than the steady state value.

The Peierls plasticity flow law (Evans and Goetze, 1979) is used for fitting the data at $T = 855$ and 1129 K. Power-law creep parameters from the literature (Kirby, 1983; Chopra and Paterson, 1984; Karato and Wu, 1993) are used to fit the stress–strain rate data at $T = 1504$ and 1780 K with V^* as 0 and $15 \text{ cm}^3 \text{ mol}^{-1}$. The parameters for the Peierls plasticity and power-law creep flow laws are listed in Table 3. The stress is calculated using the measured strain rate and the flow laws with the parameters given in Table 4. Fig. 7 illustrates the entire range of calculated stresses for the three listed flow models assuming $V^* = 0 \text{ cm}^3 \text{ mol}^{-1}$ by the brown-colored band. The calculated stress with $V^* = 15 \text{ cm}^3 \text{ mol}^{-1}$ at $T = 1504$ and 1780 K is indicated by the light green-colored band. Our data are clearly inconsistent

Table 2
Run San_36^a condition, and stress results

P (± 0.5 GPa)	T (± 10 K)	Time (± 1 s)	σ fine ^b (GPa)	$-\Delta\sigma$ fine ^c (GPa)	$+\Delta\sigma$ fine ^c (GPa)
8	25	5590	0.71	0.11	0.07
8	618	6010	1.09	0.20	0.58
8	618	6370	1.40	0.32	0.18
8	618	6740	1.46	0.35	0.19
8	855	7250	1.57	0.06	0.09
8	855	7530	1.51	0.17	0.12
8	855	7820	1.56	0.08	0.09
8	1129	8420	0.79	0.37	0.45
8	1129	8750	0.61	0.06	0.04
8	1129	9210	0.50	0.18	0.17
8	1129	9410	0.55	0.23	0.14
8	1504	9830	0.42	0.16	0.25
8	1504	10200	0.26	0.23	0.20
8	1504	10500	0.29	0.17	0.11
8	1780	11800	0.09	0.07	0.04
8	1780	12300	0.10	0.08	0.04
8	1780	12800	0.09	0.09	0.05
P (± 0.5 GPa)	T (± 10 K)	Time (± 1 s)	σ coarse ^b (GPa)	$-\Delta\sigma$ coarse ^c (GPa)	$+\Delta\sigma$ coarse ^c (GPa)
8	25	5390	0.90	0.12	0.27
8	618	6110	1.40	0.10	0.11
8	618	6480	1.48	0.26	0.12
8	618	6830	1.54	0.14	0.17
8	855	7620	1.56	0.16	0.24
8	855	7910	1.46	0.30	0.18
8	1129	8330	0.81	0.37	0.19
8	1129	8650	0.64	0.36	0.12
8	1129	9000	0.49	0.06	0.04
8	1129	9320	0.29	0.07	0.18
8	1504	9930	0.22	0.15	0.10
8	1504	10300	0.19	0.05	0.04
8	1504	10900	0.15	0.03	0.04
8	1780	11700	0.24	0.14	0.10
8	1780	12200	0.21	0.14	0.08
8	1780	12600	0.28	0.09	0.09

Note. Numbers in parenthesis indicate the one standard deviation.

^a X-ray diffraction spectra of specimens are taken at different times, that is, the stresses are measured at different time for the two specimens. Fine and coarse stand for fine- and coarse-powder specimens, respectively.

^b Stresses represent the average of stresses measured from diffraction peaks of (112), (131), (130), and (021).

^c Errors of stresses represent the range of stresses for the four diffraction peaks. The error for the stress measured from an individual peak is expected to be <0.1 GPa.

with the higher activation volume. Rather, a relatively small activation volume ($0\text{--}5\text{ cm}^3\text{ mol}^{-1}$), as derived from the silicon diffusion experiments of Bėjina et al. (1997), is consistent with the grain-size independent flow observation at the condition of 8 GPa, differential stress below 2 GPa and grain size between 0.5 and 5 μm . This activation volume is the average activation volume over 8 GPa of pressure and could be compat-

ible with the larger values that have been reported for low pressure.

We have documented the first in situ experimental strain rate and differential stress measurements in a multi-anvil press. Our results give the direct evidence for a relatively small activation volume for dislocation creep in dry olivine. These data must be taken as qualitative until the transient phenomena associated

Table 3
Flow laws

Peierls plasticity: $\dot{\epsilon} = \dot{\epsilon}_0 \exp\left(-\frac{Q_d}{RT}\left(1 - \frac{\sigma}{\sigma_0}\right)^2\right)$	
San Carlos Peridotite (Evans and Goetze, 1979)	
$\sigma_0 = 9.1$ GPa	Peierls stress
$\dot{\epsilon}_0 = 1.3 \times 10^{12}$ s ⁻¹	Reference strain rate
$Q_d = 498$ kJ mol ⁻¹	Activation energy
σ	Stress
$\dot{\epsilon}$	Strain rate
Power law creep: $\dot{\epsilon} = A\sigma^n \exp\left(-\frac{E^* + PV^*}{RT}\right)$	
A	Material constant
E^*	Activation energy
V^*	Activation volume
n	Stress exponent
R	Gas constant, 8.3144 J mol ⁻¹ K ⁻¹

Table 4
Parameters for power law creep

Dry olivine	Flow law 1	Flow law 2	Flow law 3
A	6.31E-17 ^a (MPa ⁻ⁿ s ⁻¹)	3.50E+22 ^b (s ⁻¹)	4.85E+04 ^c (MPa ⁻ⁿ s ⁻¹)
n	3.5 ^a	3.5 ^b	3.5 ^c
E^* (J mol ⁻¹)	5.33E+05 ^a	5.40E+05 ^b	5.35E+05 ^c
V^* (cm ³ mol ⁻¹)	0 and 15	0 and 15	0 and 15

^a Kirby (1983).

^b Karato and Wu (1993), the value for A is obtained by normalizing stress to shear modulus in the flow law.

^c Chopra and Paterson (1984).

with the relaxation style experiments are fully understood. The present study demonstrates that the in situ experimental studies of plastic deformation of mantle minerals at mantle pressures are possible. Our new techniques should be able to contribute to a better understanding of the dynamics of the Earth's deep interior.

Acknowledgements

The authors thank SAM group (especially Liping Wang) for providing technical support, Zhenxian Liu for his support at the beam line U2A of the National Synchrotron Light Source (NSLS), and Zhong Zhong for his support at the NSLS beam line. This research was carried out at the NSLS, which is supported by the U.S. Department of Energy, Division of Material Sciences and Division of Chemical Sciences under contract no. DE-AC02_98CH10886. Operations of the beam lines X17 and U2A are supported by COM-

PRES (EAR0135554). This research was supported by the NSF Grant EAR-9909266, EAR0135551, and EAR0229260 and the Centre National de la Recherche Scientifique (CNRS). MPI publication no. 313.

References

- Béjina, F., Raterron, P., Zhang, J., Jaoul, O., Liebermann, R.C., 1997. Activation volume of silicon diffusion in San Carlos olivine. *Geophys. Res. Lett.* 24, 2597–2600.
- Borch, R.S., Green II, H.W., 1987. Dependence of creep in olivine on homologous temperature and its implications for flow in the mantle. *Nature (Lond.)* 330, 345–348.
- Brodholt, J., Stein, S., 1988. Rheological control of Wadati–Benioff zone seismicity. *Geophys. Res. Lett.* 15 (10), 1081–1084.
- Chopra, P.N., Paterson, M.S., 1984. The role of water in the deformation of dunite. *J. Geophys. Res.* 89, 7861–7976.
- Evans, B., Goetze, C., 1979. The temperature variation of hardness of olivine and its implication for polycrystalline yield stress. *J. Geophys. Res.* 84, 5505–5524.
- Green, H.W., Borch, R.S., 1987. The pressure dependence of creep. *Acta Metall.* 35, 1301–1315.
- Hirth, G., Kohlstedt, D.L., 1996. Water in the oceanic upper mantle implications for rheology, melt extraction and the evolution

- of the lithosphere. *Earth Planet. Sci. Lett.* 144 (1–2), 93–108.
- Isaak, D.G., 1992. High-temperature elasticity of iron-bearing olivines. *J. Geophys. Res. B: Solid Earth and Planets* 97 (2), 1871–1885.
- Jaoul, O., Houlter, B., Abel, F., 1983. Study of (super 18) O diffusion in magnesium orthosilicate by nuclear microanalysis. *J. Geophys. Res. B* 88 (1), 613–624.
- Karato, S.-I., Rubie, D.C., Yan, H., 1993. Dislocation recovery in olivine under deep upper mantle conditions implications for creep and diffusion. *J. Geophys. Res. B: Solid Earth Planets* 98, 9761–9768.
- Karato, S.-I., Wu, P., 1993. Rheology of the upper mantle a synthesis. *Science* 260, 771–778.
- Kirby, S.H., 1983. Rheology of the lithosphere. *Rev. Geophys. Space Phys.* 21, 1458–1487.
- Kohlstedt, D.L., Chopra, P.N., 1994. Influence of basaltic melt on the creep of polycrystalline olivine under hydrous conditions magmatic systems. *Int. Geophys. Ser.* 57, 37–53.
- Kohlstedt, D.L., Nichols, H.P.K., Hornack, P., 1980. The effect of pressure on the rate of dislocation recovery in olivine. *J. Geophys. Res.* 85 (B6), 3122–3130.
- Kohlstedt, D.L., Wang, Z., 2001. Grain-boundary sliding accommodated dislocation creep in dunite. *Eos. Trans. AGU* 82 (47), F1137.
- Li, L., Raterron, P., Weidner, D., Chen, J., 2003. Olivine flow mechanisms at 8 GPa. *Phys. Earth Planet. Interior* 138 (2), 113–129.
- Poirier, J.P., 1985. *Creep of Crystals, High-Temperature Deformation Processed in Metals, Ceramics and Minerals.* Cambridge University Press, Cambridge, pp. 63–75.
- Ross, J.V., Ave Lallemand, H.G., Carter, N.L., 1979. Activation volume for creep in the upper mantle. *Science* 203 (4377), 261–263.
- Singh, A.K., Balasingh, C., Mao, H.-K., Hemley, R., Shu, J., 1998. Analysis of lattice strains measured under nonhydrostatic pressure. *J. Appl. Phys.* 83 (12), 7567–7575.
- Vaughan, M.T., et al., 1998. T-cup: a new high-pressure apparatus for X-ray studies. *Rev. High Pressure Sci. Technol.* 7, 1520–1522.
- Weidner, D.J., 1974. Rayleigh wave phase velocities in the Atlantic Ocean. *The Geophys. J. Royal Astronom. Soc.* 1 (1), 105–139.
- Weidner, D.J., 1998. Rheological studies at high pressure. *Rev. Mineral. Ultrahigh-Pressure Mineral.* 37, 493–522.
- Weidner, D.J., et al., 1992. Characterization of stress, pressure, and temperature in SAM85, A DIA type high pressure apparatus. In: Syono, Y., Manghnani, M.H. (Eds.), *High-Pressure Research: Application to Earth and Planetary Sciences.* Terra Scientific Publishing Company and American Geophysical Union, Tokyo and Washington, DC, pp. 13.
- Zha, C.-S., Duffy, T.S., Downs, R.T., Mao, H.-K., Hemley, R.J., 1996. Sound velocity and elasticity of single-crystal forsterite to 16 GPa. *J. Geophys. Res. B: Solid Earth Planets* 101 (8), 17535–17545.